# Towards Dynamic Holographic Laser Beam Shaping

Marcus BAUM[*1,2], Peter BECHTOLD[*1,2], Johannes STRAUSS[*1,2], Michael SCHMIDT[*1,2]

[*1] *Institute of Photonic Technologies, Friedrich-Alexander-Universität Erlangen-Nürnberg, Konrad-Zuse-Str. 3/5, 91052 Erlangen, Germany*
*E-mail: info@lpt.uni-erlangen.de*
[*2] *Erlangen Graduate School in Advanced Optical Technologies (SAOT), Friedrich-Alexander-Universität Erlangen-Nürnberg, Paul-Gordan-Str. 6, 91052 Erlangen, Germany*

High-power ultrashort pulsed lasers with average powers exceeding 100 W are commercially available. Yet, the successful transfer of such lasers into application, microstructuring in particular, lacks appropriate tools. The most promising strategies today are high-speed beam scanning or parallelization in terms of beam shaping or multi-spot generation. A combination of both strategies into one device would be the most promising tool to reach much higher processing efficiencies compared to date. We will present the first sub-steps we are undertaking to realize such devices, utilizing the acoustooptic effect as well as liquid crystal based modulators and phase holograms. First results include the rapid manufacturing of phase holograms and high-speed beam scanning and shaping using acoustooptical deflectors – reaching beam shape switching times of 1 µs.
DOI: 10.2961/jlmn.2015.02.0020
**Keywords:** Beam shaping, holography, spatial light modulator, acoustooptic, ultrashort, ITO

## 1. Introduction and Motivation

The average power of ultrashort pulsed lasers increased significantly over the past years. Commercial laser systems reach 400 W of average output power (at 15 MHz repetition rate) [1], scientific laser systems more than 1 kW (at 10 MHz repetition rate) [2,3]. In principal, this would allow a significant increase of processing speed. But when transferring such laser systems into microstructuring as application, two typical conditions have to be met:

Firstly, the maximum applicable pulse energy is limited, because melting of the surface layer takes place at too high pulse energy [4] and feature size may exceed the target range, especially when Gaussian beam intensity profile is used.

Secondly, the maximum applicable repetition rate is limited, because pulse-plasma interaction and heat accumulation take place at repetition rates exceeding approximately 100 kHz [5] if lateral pulse-to-pulse separation is not sufficiently high [6]. The applicable repetition rate is directly dependent on the laser beam scanning system and limited to 1 MHz in case of galvanometer scanners and NIR wavelength range [7].

To overcome one or the other condition, high-speed beam scanning [6] or process parallelization – in terms of beam profile shaping [8–11] – is applied. Still, several 100 W of ultrashort pulsed laser power are not yet efficiently coupled into application.

To overcome the explained limitations, our efforts aim towards a combination of high-speed beam scanning with dynamic (i.e. pulse-to-pulse) beam profile shaping, which we refer to as dynamic holographic laser beam shaping. The state of the art for such systems is the Liquid Crystal Spatial Light Modulator (LC-SLM), with which first promising results were achieved. However the SLM is limited to laser power below approximately 50 W, VIS or NIR wavelength range and rather slow frame rate of ~ 100 Hz. In the following, we will show and summarize our first steps towards different and novel technologies for dynamic holographic laser beam shaping, which will reach > 1 MHz frame rate and/or be suitable for > 100 W of laser power.

## 2. Rapid manufacturing of diffractive optical elements with high damage threshold

First, we briefly demonstrate the capabilities of holographic laser beam shaping by LC-SLM for laser structuring applications. In our setup, we used a picosecond laser (Time Bandwidth Fuego) at a wavelength of 532 nm with a pulse duration of 10 ps. A typical experimental setup is shown in Fig. 1. The raw beam is expanded by a telescope to overfill the active area of the SLM (Hamamatsu, X10468-04). The active area of the SLM is now imaged onto the entrance aperture of a microscopy objective. The sample is placed in the focal plane of the objective. A camera behind a dichroic mirror is used to monitor the structuring progress and allows aligning of the sample to the focal plane [12]. The wavefront of the laser beam is shaped by the phase pattern (also called computer generated hologram (CGH) displayed on the SLM. The microscope objective focuses the incident wave front amplitude, which leads to an intensity distribution in the focal plane according to the Fourier transformation of the incident wave front amplitude. An exemplary micro structure generated by this approach on stainless steel is shown in Fig. 2. Here, the contour of the letters “LPT” is structured using only a single CGH. The width of the lines is approximately 10 µm. This example shows the capabilities of holographic beam shaping for applications in laser based micro structuring.

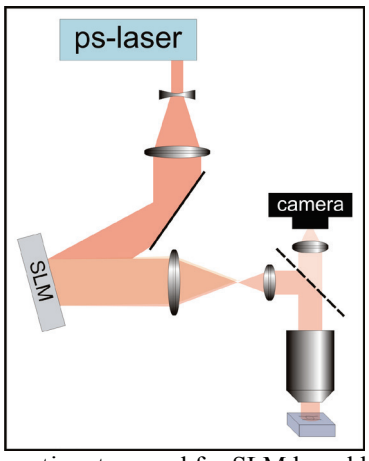


Fig. 1. Schematic setup used for SLM based holographic microstructuring

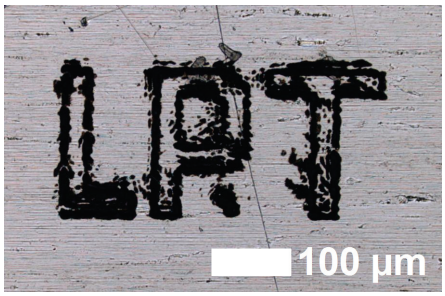


Fig. 2. Optical microscope image of a microstructure generated by SLM beam shaping. The sample material used was 1.4301 stainless steel.

However, the damage threshold in matters of laser power of commercially available SLM systems is typically a few watts. Thus in the following we present a different approach, in which we use fixed phase masks for beam shaping. These masks are generated by laser ablation of ITO nanoparticle layers [13] in a rapid manufacturing fashion.

### 2.1 Rapid manufacturing of phase holograms

In the presented experiments, we used ITO nanoparticles with a primary particle size of 20 nm. We dispersed these particles in ethanol at a 20 wt% loading while we stabilized the dispersion by addition of 3 wt% trioxadecanoic acid. According to dynamic light scattering measurements, the suspension displays a particle size distribution ranging from 20 nm to 120 nm. A more detailed description of the preparation of the suspensions can be found in [14]. In a next step, we produce particle layers of uniform thickness by spin-coating of the particle suspensions on soda-lime glass substrates with a dimension of 26 x 26 mm. In this process we deposited 200 µl of the suspensions on the glass substrates and spun them at 3000 rpm for 20 s. We measured the surface roughness as well as the thickness of the generated layers with a laser scanning microscope (Olympus Lext OLS4000). For the determination of the layer thickness we induced scratches on the sample surface and analyzed the profile of these scratches. For laser ablation of the layers we used the aforementioned ps-laser at a wavelength of 355 nm and a repetition rate of 200 kHz. The laser was guided over the sample surface by a galvo-scanner (Scanlab GmbH Intelliscan) with a focal length of 100 mm and a nominal spot size of 12 µm. The scanner system was synchronized to the laser using a delay generator (Stanford Research Systems DG645).

When light is guided through a transparent material, its phase is shifted. The phase shift φ of light transmitted through an ITO particle layer with a thickness d in comparison to light transmitted through air can be calculated by

$$\varphi = 2\pi d\left(n_\lambda - 1\right)/\lambda . \qquad (1)$$

The real part of the effective refractive index of the particle layer $n_\lambda$ needed in this calculation is shown in Fig. 3. The acquisition of the shown data by ellipsometry is described elsewhere [9]. In order to generate a binary phase hologram designed for a read-out wavelength of 532 nm, the ITO layer thickness needs to introduce a phase shift of π, which corresponds to d = 540 nm according to equation 1. By spin coating we generated a particle layer with approximately this thickness.

We also evaluated the refractive index of the soda-lime substrate by ellipsometry (see Fig. 3). As it displays similar values as the ITO layer in the visible wavelength range, reflections arising from the interface at the glass / particle layer can be neglected. Since the particle layer shows a very high optical transmission of about 90 % [9,15] while at the same time it can be ablated from the glass substrate free of residues by focused ultrashort pulsed laser irradiation [16] it is possible to generate a structure introducing a phase shift only to visible light transmitted through the layer.

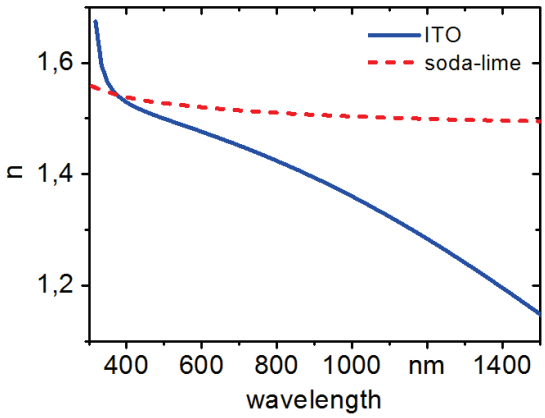


Fig. 3. Real part of the effective refractive index of the particulate ITO layer material [9] (continuous blue line) as well as the refractive index of the soda-lime substrate (dashed red line) acquired by spectroscopic ellipsometry.

We used the software VirtualLab to calculate a binary hologram with a lateral dimension of 1000 by 1000 pixels and a phase shift of π (The desired intensity distribution is shown in the inset of Fig. 5). This hologram pattern was then transferred to the particle layer by laser ablation of the particle layer.

To do so, single laser pulses with a pulse energy of 1.1 µJ were used to ablate each pixel, where a phase shift is desired. With the synchronized scanner we achieved a structuring speed of approximately $166 \cdot 10^3$ pixels/s. I.e. the hologram was produced in 6 seconds only.

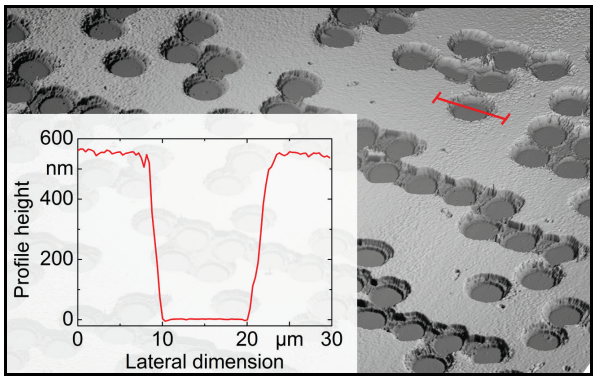


Fig. 4. LSM image of a small fraction of the sample surface after laser structuring. The inset shows the height profile along the red line in the image.

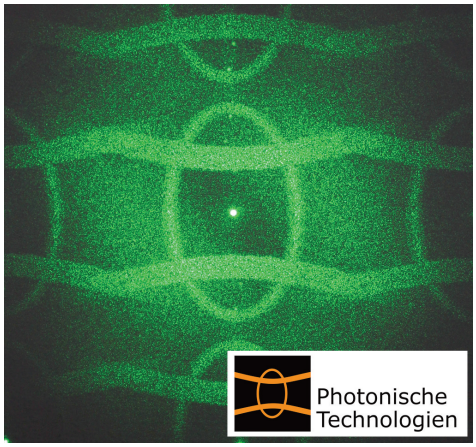


Fig. 5 Photograph of the diffraction pattern generated by the hologram on a white screen placed perpendicular to the incident beam.

An exemplary area of the generated hologram is shown in Fig. 4. The inset of Fig 4 shows the ablation profile of one of the pixels. The smooth bottom of the ablation indicates the residual free removal of the particle layer. Thus we expect defined phase shifts for the transmitted light.

Next, we placed the hologram in the collimated beam of a diode pumped frequency doubled Nd:YAG laser with a wavelength of 532 nm and a power of 11 mW. The generated diffraction pattern on a white screen perpendicular to the beam is shown in Fig. 5. It is immediately apparent that the diffraction pattern excellently resembles the desired pattern shown in the inset of Fig. 5. Evaluation of the diffraction pattern revealed that only 6.3 % of the transmitted power is going to the $0^{th}$ order in the center of the diffraction pattern. We are currently working on reducing the diffusely scattered part of the light distributed over the whole pattern by shaping of the structuring beam. We expect that more defined ablations will further increase the contrast in the diffraction pattern while the zero order intensity will be further reduced.

The presented layers show an ablation threshold on the order of 0.6 J/cm$^2$ for picosecond laser pulses. Thus we expect a significant durability for cw applications.

In order to further increase the applicability of the generated phase holograms especially for high power applications, their durability in terms of the ablation threshold can be significantly increased by thermal annealing [17] as well as by laser consolidation of the nanoparticles which was demonstrated in [15,17]. Fig. 6 shows the surface of a nanoparticle layer after consolidation by irradiation with a 248 nm excimer laser pulse. The layer density significantly changes during this consolidation step. Thus, most likely the effective refractive index of the layer will increase noticeably due to a decrease in layer porosity i.e. an increase in layer density. At the same time, the optical path length of light traveling through the layer stays unchanged as the layer thickness decreases equally. Thus, the function of the hologram will likely be fully preserved.

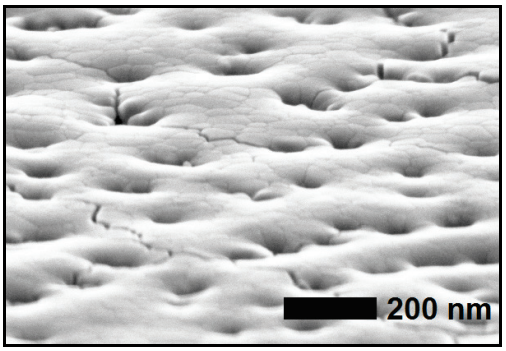


Fig. 6. SEM image of an ITO layer surface after excimer laser consolidation.

## 3. Beam shaping using acoustooptical deflectors

The results presented in section 2 aimed for beam shaping of high-power laser beams. As stated in the introduction, we are investigating possibilities to combine this characteristic with dynamic changes to the phase mask -- comparable to SLMs, but on a much faster scale. One method utilizes the acoustooptical effect in conjunction with synchronizing the acoustic signal to the emission of ultrashort laser pulses.

When an ultrashort laser pulse transmits an acoustooptical deflector (AOD), it is affected by a standing acoustic grating in approximation, because the speed of sound in the AOD material, with which the acoustic grating transverses the acoustooptical crystal, is much lower than the speed of light in the crystal. Calculations with typical values result in a propagation distance of the acoustic wave of ~100 nm, whereas the typical acoustic grating spacing is > 5 µm [18]. To date, acoustooptical scanning was realized by using constant acoustic frequency gradient in time (df/dt) as acoustic control signal, which induces a cylinder lensing effect [19]. The consideration of a standing acoustic grating to act on an ultrashort laser pulse suggests that acoustooptical beam scanning and shaping may also be realized with arbitrary frequency signal forms, such as frequency-stepping.

To demonstrate this principle we realized cylinder-lens-free scanning of a laser beam without additional compensation optics by synchronizing frequency jumps to the pulse-pause in between two laser pulses [18]. The experimental setup we used for this and for the beam shaping presented in section 3.1 is shown in Fig. 7. When a laser pulse enters the system, the photodiode triggers an FPGA controlling the frequencies, which are then induced as acoustic waves into the two orthogonally aligned AODs. The specifications

of the ultrashort pulsed laser and AODs used in the following experiments are stated in Table 1.

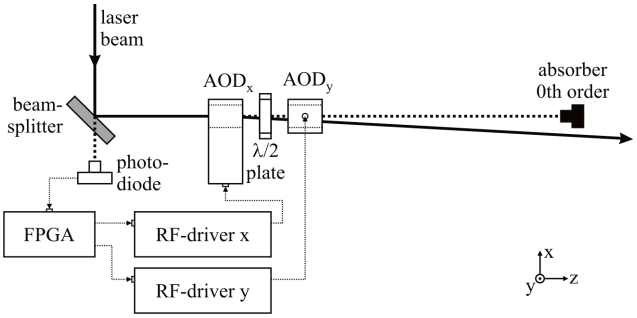


Fig. 7. Setup for acoustooptical beam scanning and shaping.

**Table 1** Specifications of the fs laser and the acoustooptical deflector

| | |
|---|---|
| **fs laser** | |
| Wavelength | 355 nm |
| Pulse duration | 300 fs |
| Repetition rate | 1 MHz |
| Pulse energy | 0.2 µJ |
| 1/e² beam diameter | 2.7 mm |
| **AOD** | |
| Material | Crystal quartz |
| Aperture | 5x5 mm² |
| Ac. Frequency | 100 MHz ... 150 MHz |
| Deflection angle | 6.2 mrad ... 9.2 mrad |
| Resolvable spots | 34 |

When using this setup as sole beam deflector (df/dt = 0 during laser pulse transit), no cylinder lensing effect is observed, compare Fig. 8b, in which the unfocussed laser beam is deflected to two alternating positions. Note that without proper synchronization, the laser beam is heavily distorted, compare Fig. 8c. The achievable beam scanning velocity is approximately 10-fold the maximum velocity of a Galvo scanner (resolvable spot rate: 34 * 1 MHz = 34 $10^6$ 1/s, Galvo scanner typ. 3 $10^6$ 1/s [7]).

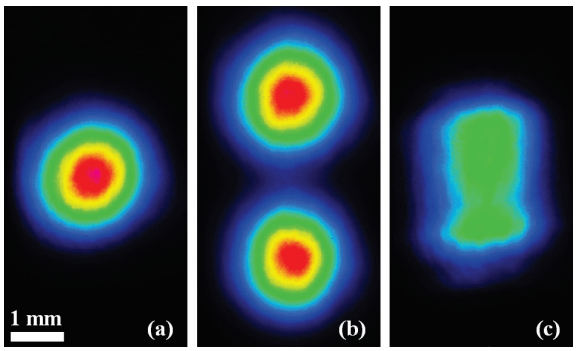


Fig. 8. Beam profiles after cylinder-lens-free acoustooptical scanning, captured at a distance of 1.7 m. (a) No scanning (f = 125 MHz), (b) Alternating deflection to +/- 0.9 mrad (110 MHz, 140 MHz) @ 1800 rad/s. (c) Equivalent to (b) but without proper synchronization.

### 3.1 Method and simulation of AOD beam shaping

Whereas up to now the frequency gradient in time was set df/dt = 0 for both x and y axis, beam shaping is achieved for df/dt ≠ 0. The spatial acoustic grating frequency $df_x/dx$ (reciprocal of acoustic grating spacing) correlates to the frequency gradient $df_x/dt$ and the deflection angle $\theta_x$ as [19]

$$\frac{d\theta_x}{dx} = \frac{\lambda}{V}\frac{df_x}{dx} = \frac{\lambda}{V^2}\frac{df_x}{dt} \tag{2}$$

(y-axis equivalently). Integrating Eq. (2) over x (or y) for a time instant and setting $\theta_x(x = 0) = 0$ ($\theta_y(y = 0) = 0$) allows to calculate the Optical Path Difference (OPD) after deflection as

$$\begin{aligned} &OPD(x,y) = x\tan(\theta_x(x)) + y\tan(\theta_y(y)) \approx \\ &\approx \frac{\lambda}{V}\left(x\cdot f_x(x) + y\cdot f_y(y)\right) \end{aligned}, \tag{3}$$

where OPD(0,0) is chosen to be 0 for the center points of the AOD apertures x = y = 0 [18]. Fig. 9 schematically shows the OPD in relation to the deflection and an exemplary wavefront shaping with a single frequency jump in the middle of the aperture.

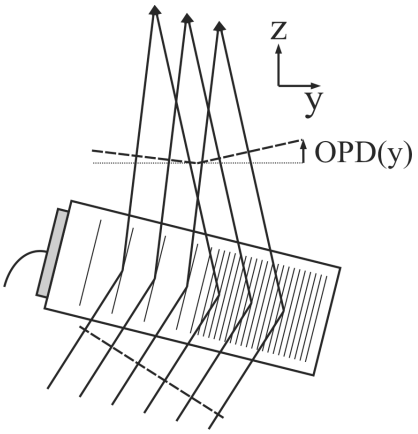


Fig. 9. Exemplary shaping of the Optical Path Difference (OPD) by an acoustic frequency jump

Note that in Eq. (3) both the x- and y-AOD were considered. As is well known, a given OPD (or phase function) may be used to calculate the intensity profile in the focus of a lens via Fourier transformation. To simulate the resulting beam profile, we used the Fast Fourier Transformation as described in [20] in a simplified way with

$$\begin{aligned} &I_f(x',y') \sim \left|FFT\left(\sqrt{I_0(x,y)}\cdot\exp\left(i\frac{2\pi}{\lambda}OPD(x,y)\right)\right)\right|^2, \\ &x' = x\frac{\lambda fN}{b^2};\ y' = y\frac{\lambda fN}{b^2}; \end{aligned} \tag{4}$$

where $I_f$ and $I_0$ are the relative intensities in the object (0) and focus plane (f) and N is the number of samples along the height / length b of the sampling window in the object plane. For $I_0$ we use a Gaussian intensity distribution of 1/e² diameter $2w_0$. Note that we always normalize $I_0$ and $I_f$ to 1, hence we are showing relative intensities in the results.

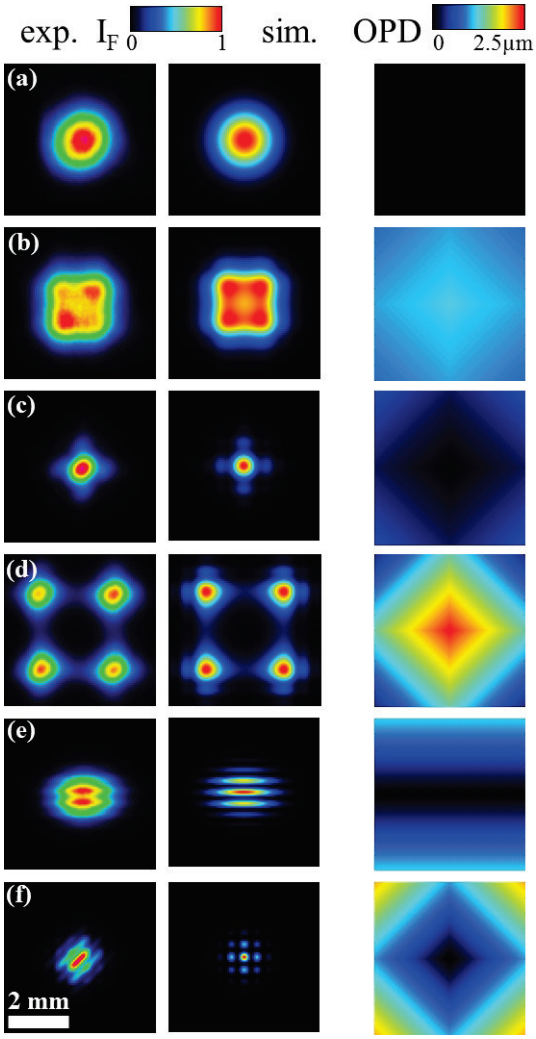


Fig. 10. Left column: experimental beam profiles after acoustooptical beam-shaping via frequency switching; middle column: simulation of the same; right column: applied Optical Path Difference in simulation. (a) No beam shaping for reference, (b) Divergence with -60 µrad, (c) Convergence with +120 µrad, (d) Beam splitting with -420 µrad, (e) Interference pattern with +480 µrad in y-axis, (f) Interference pattern with +420 µrad in both axes.

### 3.2 Demonstrative results of beam shaping via acoustic frequency switching

For beam shaping via acoustic frequency shifting we are using the same setup as shown in Fig. 7. In difference to before, the frequency jump is now synchronized to the laser pulse emission in such way, that the spatial frequency jump (i.e. the change of the acoustic grating spacing) is in the middle of the AOD aperture, when the laser pulse transmits the AOD. Hence, the unfocussed beam profile is first split into two sections along the x-axis, compare Fig. 9, and then the same for the y-axis. The deflection of the sections is now controlled independently of each other. In this way, rudimentary beam shaping is achieved.

Fig. 10 shows the resulting beam shapes of an unfocussed beam after shaping with the afore described method and 1.7 m behind the acoustooptical deflectors. To verify the experimental results we used Eq. (4) in conjunction with Eq. (3) to directly calculate the resulting beam shapes of the unfocussed beam without any additional correction terms. As Eq. (4) will calculate the beam shape in the focus of a lens with focal length f = 1.7 m (i.e. $2w_f = 0.28$ mm), we introduce a defocussing term as Zernike polynomial $Z_4$ (defocus) with $(2f)^{-1}(x^2 + y^2) = -0.29$ 1/m $(x^2 + y^2)$, so that without shaping $2w_f \approx 2w_0 = 2.7$ mm. By doing so, we are not calculating the beam profile of a focused laser beam but for the collimated laser beam as intended. Fig. 10 additionally shows the applied OPD without the defocussing term, i.e. the OPD, which is also applied experimentally.

The results indicate an excellent accordance of experiments and simulations. When interference is induced, compare Fig. 10 (e) and (f), the simulation overestimates the contrast ratio of the interference pattern. We attribute this to the low coherence length of our fs-laser, which is approximately 10 µm or less.

It is to be noted, that Fig. (10) represents the beam profile shape of single laser pulses and that the beam profile shape is switchable from pulse to pulse at a switching time, which corresponds to the repetition rate of 1 MHz.

### 3.3 Analysis of achievable focal beam shape

With the tool of focal intensity evaluation via FFT analysis, we investigate the possibilities of freely adapting the (spatial) acoustic frequencies $f_y(y)$ and $f_x(x)$ to evaluate the benefits of such a beam shaping device.

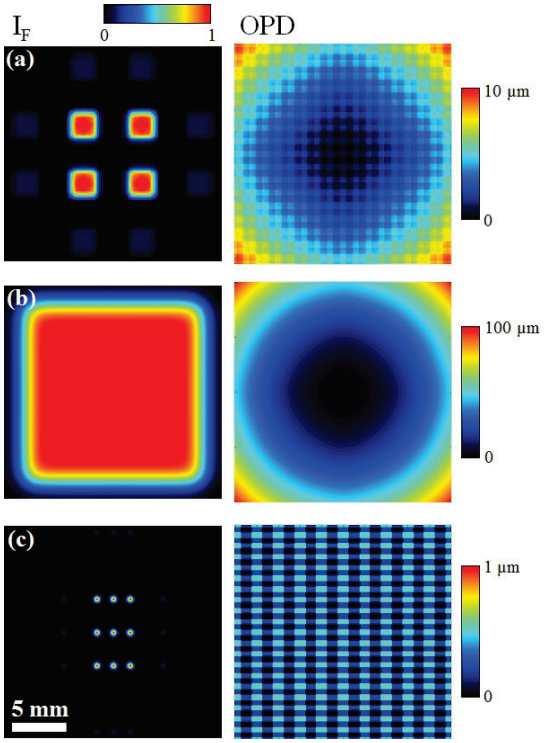


Fig. 11. Simulated beam profiles after acoustooptical beam-shaping; left: relative intensity at the focus of a 100 mm lens, right: Optical Path Difference. (a) 4x split top-hat profile, (b) enlarged top-hat profile, (c) 3x3 multi-spot array.

In regards to wavefront correction, several wavefront errors in terms of Zernike polynomials may be compensated more or less accurately, which is of great use for microscopy, for instance. We already described this in [18]. More usable in microstructuring is the reshaping to either several spots or to a top-hat beam profile. Fig. 11 shows

exemplary results of the simulations of such beam shaping. In these simulations we used $\lambda = 1$ µm, $w_0 = 5$ mm and $f = 100$ mm. The beam may be reshaped to several geometries, however reshaping is still limited to first shaping the x-axis and then the y-axis of a laser beam. This means that e.g. the rotation of the shapes 45° is not possible directly.

## 4. Outlook on further possibilities for dynamic, holographic beam shaping

For acoustooptical beam shaping, we proposed a research project, in which we are planning to investigate the possibilities of such devices experimentally and analytically. We will also look into adapting well-known optimization methods for spatial light modulators, such as the Gerchberg-Saxton or adaptive-additive algorithms [21], to this method.

Furthermore we will investigate the possibility to realize beam shaping in acoustooptical manner via refraction instead of diffraction. For this, much lower acoustic frequencies will be applied to the crystal, so that effectively no diffractive (e.g. grating) but a refractive optical element (e.g. lens) is affecting the incident laser beam. With this method, the shaping magnitude will presumably be much lower, but diffraction losses are fully avoided. Similar approaches were already successful [22,23].

Moreover, we are currently investigating the feasibility of using the plasma dispersion effect in wide-bandgap semiconductor structures for light phase manipulation. In this way the liquid crystal commonly used in SLMs can be avoided resulting in potentially high speed devices that can bear high laser powers.

## 5. Conclusion

We showed that the two major ways to improve process efficiency of high-power ultrashort pulsed lasers in microstructuring and other applications is parallelization and/or high-speed scanning. A combination of both in one device is highly preferable.

We introduced several potential solutions to achieve either parallelization or high-speed scanning or both:

- Rapid-manufactured phase masks:
  - Suitable for high-power
  - Fixed beam shape
- Diffractive acoustooptical beam shaper:
  - Suitable for high-power
  - Combination of high-speed scanning and parallelization
  - Limited beam shaping possibilities
  - Limited efficiency due to diffraction

These solutions are currently under development:

- Refractive acoustooptical beam shaper:
  - Same as diffractive, but no diffraction losses
  - Presumably limited shaping capability
- Liquid-crystal-free spatial light modulator:
  - Presumably suitable for high-power
  - Presumably high-speed beam shaping

**Acknowledgments and Appendixes**

The support of the German Research Foundation (DFG, SPP 1327) is gratefully acknowledged.

Moreover, the authors gratefully acknowledge the financial support by and scientific exchange with the Erlangen Graduate School in Advanced Optical Technologies (SAOT) by the German Research Foundation (DFG), the framework of the German excellence initiative.

**References**

[1] K. Du, W. Pfleging, Y. Lu, K. Washio, W. Hoving and J. Amako: SPIE LASE: Lasers and Applications in Science and Engineering, SPIE Proceedings" (SPIE, 2009), pp. 72020Q.
[2] P. Russbueldt, T. Mans, H. Hoffmann and R. Poprawe: Proceedings of ICALEO 2010" (2010).
[3] P. Russbueldt, T. Mans, J. Weitenberg, H. D. Hoffmann and R. Poprawe: Opt. Lett., 35, (2010) 4169.
[4] T. Häfner, Y. Reg, H. Hetzner and M. Schmidt: Proceedings of LPM2012 - the 13th International Symposium on Laser Precision Microfabrication, (2012) 1.
[5] J. König, S. Nolte and A. Tünnermann: Opt. Express, 13, (2005) 10597.
[6] S. Bruening, G. Hennig, S. Eifel and A. Gillner: Physics Procedia, 12, (2011) 105.
[7] P. Bechtold, R. Hohenstein and M. Schmidt: Opt. Lett., 38, (2013) 2934.
[8] Z. Kuang, W. Perrie, D. Liu, P. Fitzsimons, S. P. Edwardson, E. Fearon, G. Dearden and K. G. Watkins: Applied Surface Science, 258, (2012) 7601.
[9] M. Baum, I. Alexeev, M. Latzel, S. H. Christiansen and M. Schmidt: Opt. Express, 21, (2013) 22754.
[10] D. Liu, Z. Kuang, W. Perrie, P. J. Scully, A. Baum, S. P. Edwardson, E. Fearon, G. Dearden and K. G. Watkins: Appl. Phys. B, 101, (2010) 817.
[11] L. Kelemen, S. Valkai and P. Ormos: Opt. Express, 15, (2007) 14488.
[12] I. Alexeev, J. Strauss, A. Gröschl, K. Cvecek and M. Schmidt: Appl. Opt., 52, (2013) 415.
[13] M. Baum, J. Strauß, F. Grüßel, I. Alexeev and M. Schmidt: J. Opt., 16, (2014) 125706.
[14] M. Mahajeri, A. Schneider, M. Baum, T. Rechtenwald, M. Voigt, M. Schmidt and W. Peukert: Thin Solid Films, 520, (2012) 5741.
[15] M. Baum, H. Kim, I. Alexeev, A. Piqué and M. Schmidt: Appl. Phys. A, 111, (2013) 799.
[16] M. Baum, I. Alexeev, M. Latzel, S. H. Christiansen and M. Schmidt: Proc. 14th International Symposium on Laser Precision Microfabrication, (2013).
[17] F. Mikschl, M. Baum, J. Heberle, I. Alexeev and M. Schmidt: Physics Procedia, 56, (2014) 991.
[18] P. Bechtold, R. Hohenstein and M. Schmidt: Opt. Express, 21, (2013) 14627.
[19] I. Chang: IEEE Trans. Son. Ultrason., 23, (1976) 2.
[20] D. Mas, J. Garcia, C. Ferreira, L. M. Bernardo and F. Marinho: Optics Communications, 164, (1999) 233.
[21] M. J. Padgett, J. Molloy and D. McGloin: "Optical tweezers" (Taylor & Francis, 2010).
[22] A. Mermillod-Blondin, E. McLeod and C. B. Arnold: Opt. Lett., 33, (2008) 2146.
[23] S. K. Yao, D. Weid and R. M. Montgomery: Appl. Opt., 18, (1979) 446.

(Received: June 16, 2014, Accepted: April 13, 2015)